Modulation of Electrical and Thermal Conductivity in Metal-Organic Framework by Conducting Polymer

MS Thesis Report submitted towards the partial fulfillment of

BS-MS dual degree program

By

Ashwini Anandrao Jadhav

20131118

Under the guidance of

Dr. Nirmalya Ballav

Indian Institute of Science Education and Research (IISER) Pune

March 2019

Certificate

This is to certify that this dissertation entitled "**Modulation of Electrical and Thermal Conductivity in Metal-Organic Framework by Conducting Polymer** towards the partial fulfillment of the BS-MS dual degree programme at the Indian Institute of Science Education and Research, Pune represents original research carried out by **Ashwini Jadhav** at Indian **Institute of Science Education and Research, Pune** under the supervision of **Dr. Nirmalya Ballav, Department of Chemistry, Indian Institute of Science Education and Research, Pune** during the academic year 2018-2019.

Dr. Nirmalya Ballav

(Supervisor)

Associate Professor

Department of Chemistry

निर्मल्या बल्लव / Nirmalya Ballav
सहयोगी प्राध्यापक, रसायनशास्त्र / Associate Professor, Chemistry
भारतीय विज्ञान शिक्षा एवं अनुसंधान संस्थान
Indian Institute of Science Education & Research
पुणे / Pune - 411 008, India

Ashwini Jadhav

20131118

IISER Pune

DECLARATION

I hereby declare that the matter embodied in the report entitled "**Modulation Of Electrical and Thermal Conductivity in Metal-Organic Framework by Conducting Polymer**" are the results of the work carried out by me at the Department of Chemistry, IISER Pune, under the supervision of Dr. Nirmalya Ballav and the same has not been submitted elsewhere for any other degree.

Dr. Nirmalya Ballav

(Supervisor)

Associate Professor

Department of Chemistry, IISER Pune

निर्मल्या बल्लव / Nirmalya Ballav
सहयोगी प्राध्यापक, रसायनशास्त्र / Associate Professor, Chemistry
भारतीय विज्ञान शिक्षा एवं अनुसंधान संस्थान
Indian Institute of Science Education & Research
पुणे / Pune - 411 008, India

Ashwini Jadhav

20131118

IISER Pune

ACKNOWLEDGEMENTS

First of all, I would like to express my sincere gratitude to my supervisor Dr. Nirmalya Ballav for giving me the opportunity to work in his lab. I have learned many a lessons over the past year, and Sir has guided me throughout the whole journey. His timely inputs and suggestions have helped me come a long way and will continue to help me in the future as well

I am also thankful to my TAC member Dr. Shabana Khan for her guidance and inputs throughout my work. A heartfelt thank you to Mr. Rajarshi Dasgupta for helping me with my measurements every time I asked for it. I would also like to acknowledge all the faculty at IISER Pune, who have taught me and helped me expand my scientific knowledge.

All the seniors in my lab have been my to-go people at all times. A special thanks to Ms. Kriti Gupta for teaching and mentoring me throughout my project. I have learned a lot from her. I owe to immense gratitude to everyone in the lab - Plawan K Jha, Syed Zahid Hassan, Shammi Rana, Sujit Bhand, Debashree Roy, Pooja Sindhu, Vikash Kumar, Anupam Prasoon, Jainendra Singh, Ishan, Gopi, Pranay as well as all the past members who paved the way for us to work in such good conditions.

A shout out to my girl gang Shifa, Mansi, Prachi, Mukta, Shweta, Minal and many more. I have learned a lot from them and with them. Having friends like these is a true blessing and it goes without saying that I am very grateful to every one of them. A big thank you to Asheesh, Wilfred, Vimanshu, who have always been there through thick and thin to always cheer me up no matter what. I consider myself extremely lucky to have met these people

The acknowledgements would be incomplete without expressing my utmost gratitude to my family members especially my Mummy, Baba, Dee and Dada. They have been and continue to be my biggest mentors and everything I am today, I owe it all them.

Last but not the least, I would like to thank DST-INSPIRE for the fellowship through all these years. It has indeed proved very beneficial for me to pursue my dream.

Dedicated to Tai and Aba

Contents

List of Schemes and Figures

Abstract

Metal-Organic Frameworks (MOFs) are well explored candidates in numerous fields such as gas storage, separation, sensing and more, however, most of them are intrinsically insulating in nature, due to which they lag behind in the domain of energy storage devices. Herein, we have assembled polypyrrole chains inside the nanochannels of a Zr-based framework (UiO-66) leading to a million fold electrical conductivity enhancement with a value of ~10^{-2} S/cm for UiO-66_PPy, at the minimal cost of porosity loss. Notably, at the same time, thermal conductivity increment in the nanocomposite is not huge, which is usually unavoidable where electrical conductivity and thermal conductivity cooperatively reforms. The nanocomposite was then tested for supercapacitor performance and revealed a value of 130mF/cm^2 at current density of 0.2 mA/cm^2 with almost 100% retention of the value after 10k cycles.

1. Introduction

1.1 Metal-Organic Frameworks (MOFs)

Metal-Organic Frameworks (MOFs) are a class of functional materials composed of metal ions/clusters connected by organic ligands via coordinate bonds (Figure 1).[1] Due to the simultaneous presence of remarkable properties such as long-range structural order, tunability, high surface area etc., these materials have gained immense attention in the last two decades. An advantage MOFs have over other porous compounds like zeolites, porous carbons etc. is their selective nature, arising from the host-guest interactions.[2] As a result of these interactions, they are useful in applications such as gas storage and separation, sensing, catalysis, drug delivery, proton conduction, magnetism etc.[3] However, MOFs are not yet explored for their applications where electrical conductivity is a primary requirement.[4] Indeed bringing them into the semiconducting and conducting regime could make them applicable in energy storage devices, field effect transistors, thermoelectrics, etc.

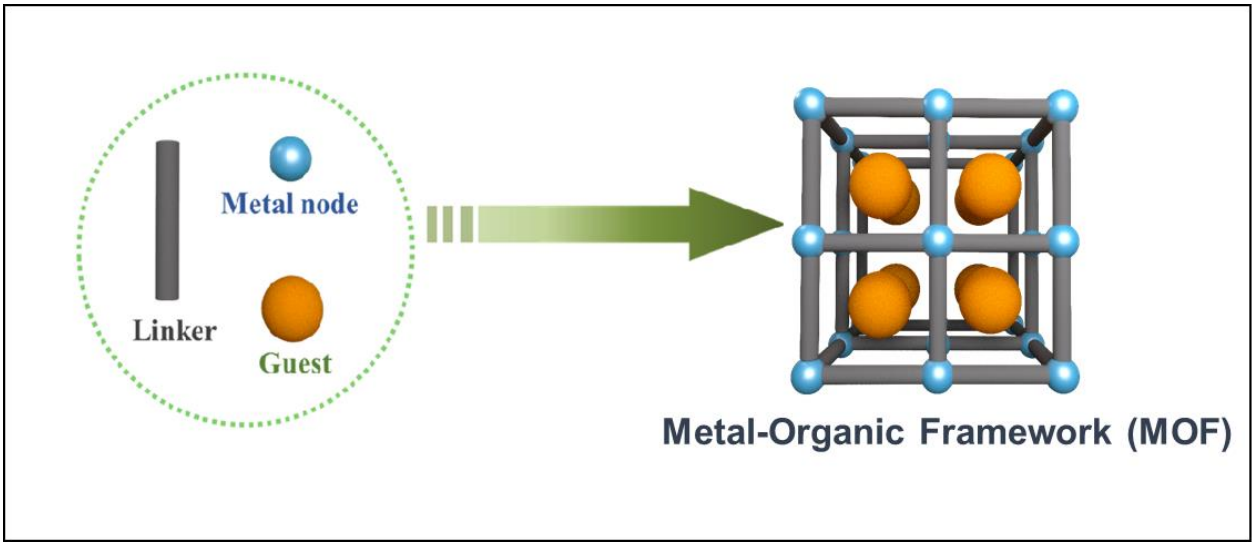

Figure 1: Schematic representing the formation of Metal-Organic Framework

1.2 Conducting Polymers

Conducting Polymers are organic polymers which are able to conduct electricity (Figure 2). Alan J Heeger, Alan Mcdarmaid, and Hideki Shirakawa received the Nobel Prize in 2000 for their discovery and development of conducting polymers.[5,6] They are characterized by the abundant availability of raw materials, low cost of production, and relatively nontoxic methods required for their synthesis. Conducting polymers, such as Aniline, Pyrrole, Thiophene, etc. can be polymerized by use of external oxidizing agents such as Iodine, transition metal salts, ammonium persulfate, and various others. Upon doping of these polymers, polaron and bipolaron bands appear which in turn reduce the band gap, making them conducting in nature.[7] Apart from the electrical conductivity aspect, they also have an interesting property showing lower values of thermal conductivity. In fact, compared to the conventional inorganic materials such as Be_2Te_3, SiGe etc. these polymers have thermal conductivity values lower than a factor of 10. Along with electrical conductivity, thermal conductivity and in turn thermoelectric properties of these polymers have been extensively studied. PEDOT-PSS, a well-known conducting polymer exhibits a thermal conductivity value of 0.17 W/mK one of the lowest values in this class of compounds.[8]

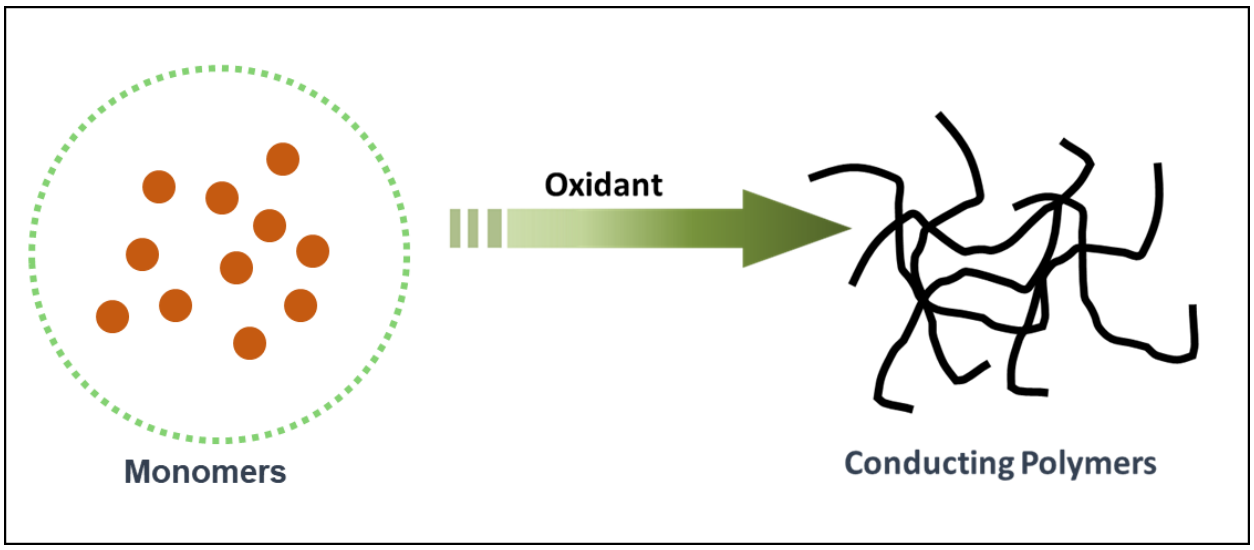

Figure 2: Schematic representing the formation of Conducting Polymer

1.3 MOF-Conducting Polymer nanocomposite

Unlike conducting polymers, MOFs are poor conductors of electricity. The reason for this is their inability to transport charge, electrons in this case, very efficiently. This is attributed to the presence of insulating organic linkers which make up the backbone of the framework, as well as the poor orbital overlap between the d orbitals of the metal centre and the s/p orbital of the ligands used.[9] In recent years, efforts have been successfully made to turn these insulating materials into semiconducting ones by different strategies such as intrinsic and extrinsic approach.[10] In the former case, the conductivity of the MOF can be modulated by changing either the metal or the ligand in the framework. As an example, upon changing the metal from Ni to Cu in a $Cu[Ni(Pdt)_2]$ MOF (Pdt = 2,3-pyrazinedithiol), the electrical conductivity is enhanced by a ~ 10^4 orders, going from 10^{-8} S/cm for $Cu[Ni(Pdt)_2]$ to 10^{-4} for $Cu[Cu(Pdt)_2]$.[11,12] In the latter case, this can be achieved by introducing external guest molecules in the voids of the framework. In 2014, Allendorf and coworkers demonstrated that the electrical conductivity in thin films of a $Cu_3(BTC)_2$ (BTC- Benzene-1,3,5-tricarboxylic acid) commonly known as HKUST-1 could be increased up to a value of 0.07 S/cm by doping of a redox active molecule TCNQ (7,7,8,8- tetracyanoquinododimethane) inside the pores.[13] Recently, there have been reports of the assembly of conducting polymers such as Polypyrrole (PPy),[14] Polyaniline (PANI),[15] Poly(3,4-ethylenedioxythiophene) (PEDOT),[16] Polythiophene (PTh)[17] etc. in the nanopores of the MOFs in order to enhance the electrical conductivity. Polymerization of the monomers in the confined nano-spaces of the framework leads to the formation of monodispersed, long, single chain polymers (Figure 3). This approach has led to the formation of MOF-conducting polymer nanocomposites which exhibit unusual physical and chemical properties due to the host-guest interactions arising out of these nanocomposites.[18] Additionally, both the MOF and the conducting polymer exhibit low values of thermal conductivity which could lead to their potential applications in thermoelectrics.[19]

However, a drawback of this approach is that the porosity of the MOF, which imparts many of the vast properties to the material, is almost always lost.[20] Retention of the porous nature along with the additional enhancement of electrical conductivity would indeed be

a plus point for these materials as the benefits of the porosity, enhanced electrical conductivity, and low thermal conductivity can be effectively utilized.

With this in mind, we have, for the first time, synthesized a porous nanocomposite made up of a chemically and thermally stable MOF, UiO-66 (Zr-BDC)[21] as the host framework and PPy as the conducting polymer. The nanocomposite retains its porous nature and exhibits enhanced electrical conductivity and lower thermal conductivity values compared to the parent MOF. To test the material for energy storage, we have fabricated a supercapacitor device using the nanocomposite and it indeed shows promising values as well as excellent capacity retention up to 10k cycles.

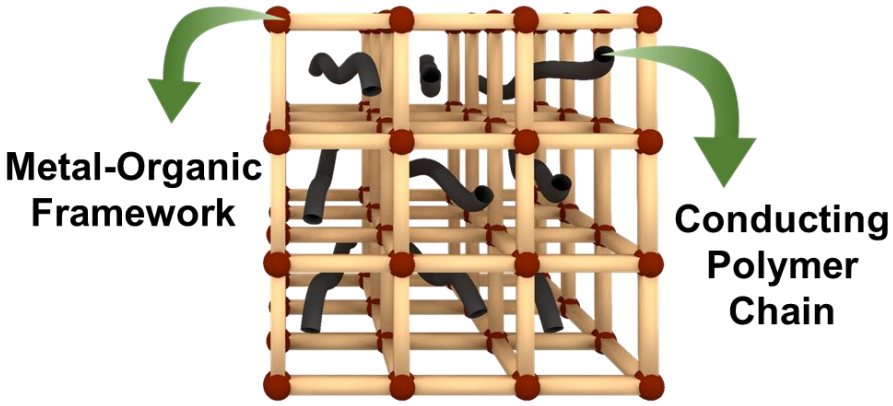

Figure 3: Schematic representing of MOF-Conducting polymer nanocomposite

2. Materials and Methods

2.1 Chemicals

$ZrCl_4$, Benzene-1,4- Dicarboxylic Acid and Pyrrole were purchased from Sigma-Aldrich. Ferric Chloride ($FeCl_3$) was purchased from CHEMLABS. *N,N*-Dimethylformamide (DMF) was purchased from RANKEM. Methanol, Water, Acetone were used as solvents.

2.1.1 Synthesis of UiO-66

UiO-66 was synthesized according to a protocol reported in the literature (Scheme 1).[22] $ZrCl_4$ (0.35 mmoles), H_2BDC (0.35 mmoles) and 4 ml *N,N*-Dimethylformamide (DMF) were sealed in a Teflon-lined autoclave and heated at 120 °C for ~24 h (Scheme 1). The obtained white product was washed with DMF and MeOH and subjected to solvent exchange by immersing it in MeOH for 7 days (MeOH was changed after every 12 h).

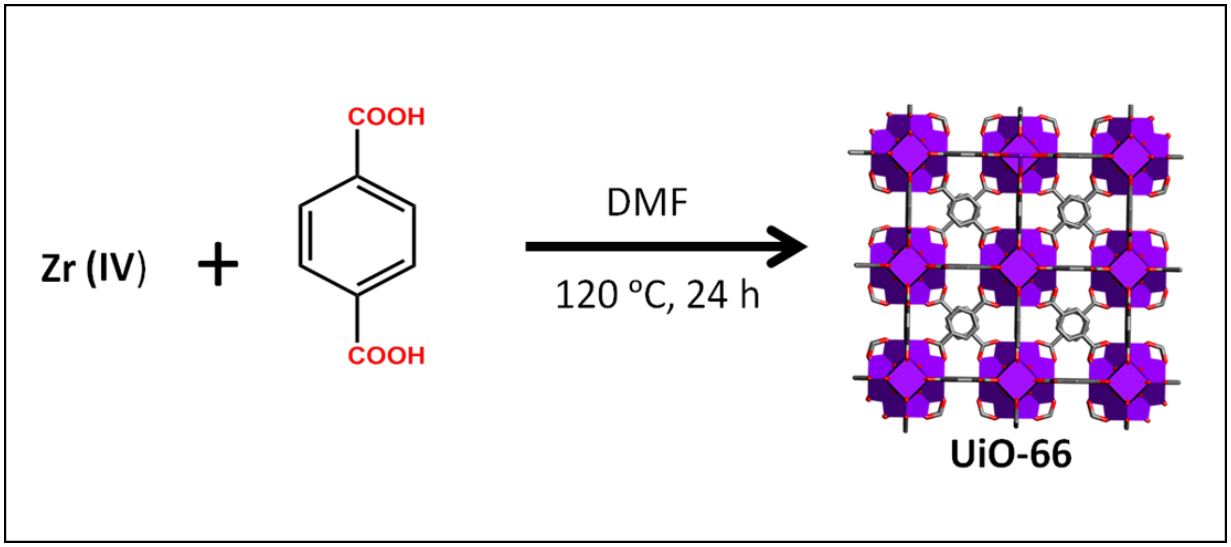

Scheme 1: Synthesis of UiO-66

2.1.2 Synthesis of UiO-66_PPy

Desolvated UiO-66 was exposed to pyrrole monomers at room temperature under N_2 atmosphere for ~48 h. The excess pyrrole was then removed by vacuum heating at 35°C for ~1 h followed by addition of aqueous $FeCl_3$ (Monomer to Oxidant ratio ≈ 1:3.5). The reaction mixture was then kept at <10 °C for ~48 h. The black powder obtained was thoroughly washed with water and MeOH followed by drying at room temperature.

2.1.3 Synthesis of bulk PPy

An aqueous solution of $FeCl_3$ (150 ml, 0.05 moles) was added dropwise to 1 ml pyrrole with continuous stirring for ~24 h. The black precipitate obtained was thoroughly washed

with water and MeOH followed by vacuum drying for ~6 h at 80 °C.

2.1.4 Activation of UiO-66

As-synthesized UiO-66 was activated at 130 °C for >6 h to remove the solvent guest molecules from the pores before all the experiments.

2.2 Supercapacitor Assembly

2.2.1 Preparation of 10 wt % PVA-H_2SO_4 electrolyte

2 g of polyvinyl alcohol (PVA) was added to 20 mL of water and stirred at 80 °C until a clear solution was obtained. This was then cooled to room temperature followed by the addition of 2 g concentrated H_2SO_4 and stirred for another 30 min.

2.2.2 Electrode fabrication of supercapacitor

~90% active material (UiO-66_PPy), ~5% conducting carbon and ~5% Nafion were mixed together using N-methyl-2-pyrrolidone (NMP) to form a uniform slurry. This slurry was drop cast on grafoil sheet (1cm x 1 cm) and dried for ~12 h at ~85 °C. These dried electrodes were then sandwiched using 10 wt % of PVA-H_2SO_4 gel electrolyte between the two electrodes. Celgard membrane was used as a separator. The loading of the active material was ~2mg/cm^2.

Electrochemical measurements in the liquid state were carried out by dipping the electrodes in 0.5M H_2SO_4, used as the electrolyte.

2.3 Characterization

PXRD was recorded on Bruker D8 Advance diffractometer with Cu Kα radiation (λ = 1.5406 Å) varying 2θ from 5 to 30°. FT-IR spectra were collected from a NICOLET 6700 spectrophotometer with KBr pellets from 400 to 4000 cm^{-1} with a resolution of 4 cm^{-1}. The gas adsorption and desorption data were collected at 77 K for N_2 gas on

Quantachrome instrument. The morphology was analyzed by using a Zeiss Ultra Plus field-emission scanning electron microscope (FESEM). HRTEM images were recorded on JEOL USA JEM-2200 FS Transmission Electron Microscope. Two-probe DC and AC conductivity measurements were done with pressed pellets sandwiched in a Swagelok cell on Keithley 2450 sourcemeter and PARSTAT MC Potentiostat PMC-2000 respectively. Four-probe measurements were done on Keithley 6221 sourcemeter. Electrochemical measurements were performed on PARSTAT MC Potentiostat PMC-2000. Solid State UV was recorded on Shimadzu UV−vis−NIR spectrophotometer (Model UV-3600 plus). Thermogravimetric analysis (TGA) and Differential Scanning Calorimetry (DSC) measurements were done using Perkin-Elmer thermal analyzer STA 6000 model and TA Q20 differential scanning calorimeter respectively. Thermal diffusivity measurements were carried out on Linses LFA 1000.

3. Results and Discussion

3.1 Characterization of UiO-66_PPy

The colour of UiO-66 changed from white to faint green upon loading of Pyrrole monomers (UiO-66_Py). On exposing UiO-66_Py to an oxidant ($FeCl_3$), this colour changed to black (UiO-66_PPy) as shown in Figure 4. The drastic colour change from white to faint green to black was understood as the primary indication of polymerization in the nanocomposite.

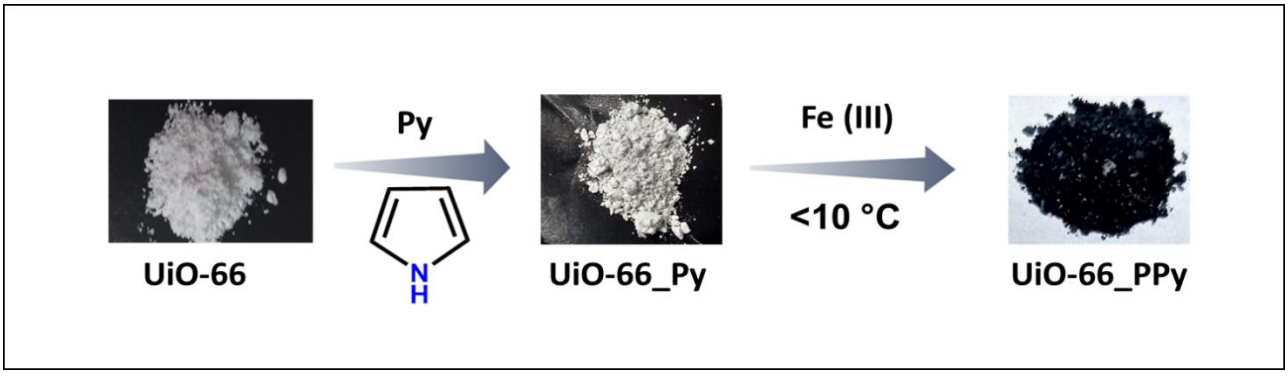

Figure 4. Optical images of UiO-66, UiO-66_Py and UiO-66_PPy

The polymerization of pyrrole occurs via oxidative polymerization method by the mechanism described below (Figure 5)[23]:

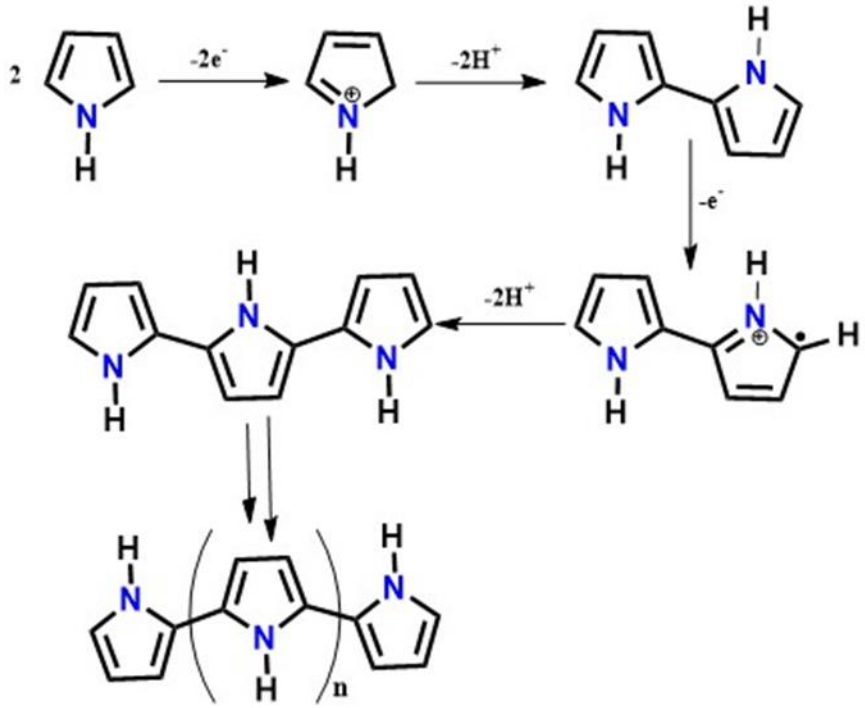

Figure 5: Mechanism for oxidative polymerization of pyrrole

To monitor how the polymerization varies with time, we carried out the reaction for 24 h, 48 h and 72 h. It was seen that a uniformly black coloured product formed in all three cases. However, with an increase in the reaction time, we observe changes in the morphology of the nanocomposite (Figure 6). In case of polymerization carried out for 72 h, formation of excess polypyrrole on the surface is observed. Taking this into account, all the further reactions were done for 48 h.

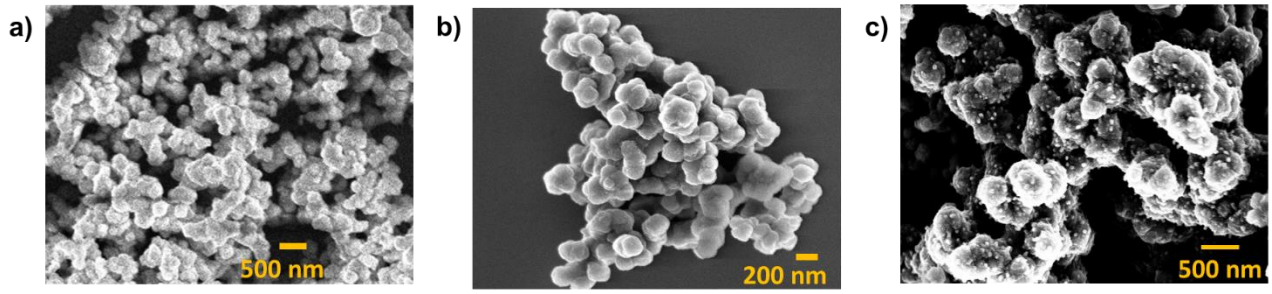

Figure 6: FESEM showing the changes in morphology of UiO-66_PPy after (a) 24 h polymerization (b) 48 h polymerization and (c) 72 h polymerization

Zr being one of the most oxophilic metals,[24] forms very strong bonds with the oxygen from the terephthalic acid linker, imparting high stability to the overall framework. The PXRD patterns of UiO-66, UiO-66_Py and UiO-66_PPy are similar, clearly indicating the retention of structural integrity of the framework after the incorporation of Polypyrrole chains. (Figure 7a). Thermogravimetric analysis (TGA) plot reveals that both UiO-66 and UiO-66_PPy are stable up to ~350 °C (Figure 7b). The initial drop up to ~100 °C is due to the loss of solvent molecules in UiO-66. In the case of UiO-66_Py, this drop corresponds to excess of monomers adsorbed on the surface of the framework. It is followed by ~15% loss attributed to the incorporation of pyrrole inside the nanopores as indicated by the red arrow in TG profile.

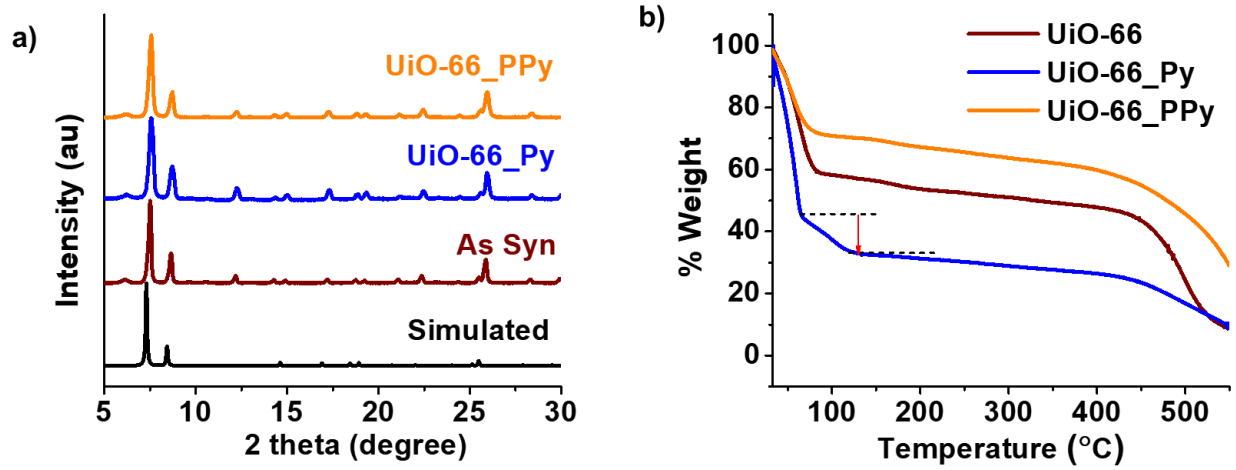

Figure 7: (a) PXRD patterns for MOF - simulated (black), UiO-66 (wine), UiO-66_Py(blue), UiO-66_PPy(orange); (b) TGA for UiO-66 (wine), UiO-66_Py (blue) and UiO-66_PPy (orange)

Furthermore, FT-IR spectra of both UiO-66 and UiO-66_PPy have peaks at ~1400 cm^{-1}, ~1582 cm^{-1} and ~748 cm^{-1} corresponding to the in and out of phase stretching of the carboxylate group and C-H wagging mode, respectively (Figure 8a). The peak at ~1017 cm^{-1} is due to the aromatic ring breathing motion of the framework.[25] Additionally, peaks at ~524 cm^{-1}, ~630 cm^{-1} and ~745 cm^{-1} can be assigned to Zr-O_2 groups in the framework. The absence of a prominent peak at ~1667 cm^{-1} (C=O stretching of DMF) successfully shows that the DMF in the framework has been replaced by MeOH during the solvent exchange process.[21] The characteristic peaks for the fundamental vibration of pyrrole rings at ~1458 cm^{-1} and ~1545 cm^{-1} appear in both UiO-66_PPy as well as externally synthesized bulk PPy. The peak at ~964 cm^{-1} is assigned to stretching vibration of doped state of PPy. The C-N stretch vibration at ~1172 cm^{-1} was also observed for UiO-66 and bulk PPy which is consistent with the values reported for Polypyrrole. These features are absent in UiO-66 as shown in the zoomed in view in (Figure 8b and 8c), thus confirming the formation of UiO-66_PPy nanocomposite.[26]

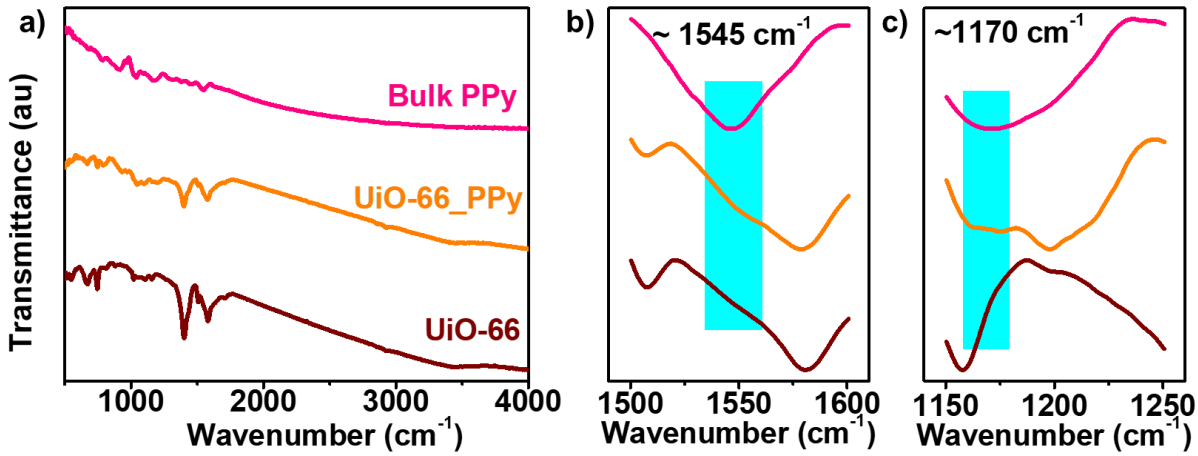

Figure 8: FT-IR spectra of (a) UiO-66 (wine), UiO-66_PPy (orange) and bulk PPy (pink). Zoomed view for peak visualization for (b) pyrrole ring stretching (c) C-N stretching of Polypyrrole.

UiO-66 is composed of two kinds of pores comprising of diameters of ~8 Å and ~11 Å interconnected to each other.[27] N_2 gas adsorption-desorption isotherms show type I behaviour for both UiO-66 and UiO-66_PPy with almost no hysteresis (Figure 9). Interestingly, UiO-66_PPy also shows a significant amount of gas uptake, although not as high as UiO-66. This decrease in the gas uptake for UiO-66_PPy is due to the formation of polymer chains, however, since the nanopores are large enough, there is still enough space to accommodate the incoming N_2 gas molecules. We calculated BET surface area form the gas adsorption data and it is found that the UiO-66_PPy exhibits a value of ~750 m^2/g which is less than value of UiO-66 whose surface area is ~1165 m^2/g. This further proves that some of the accessible surface area of the framework is lost confirming that the polymer chains have indeed been incorporated inside the nanochannels of UiO-66.

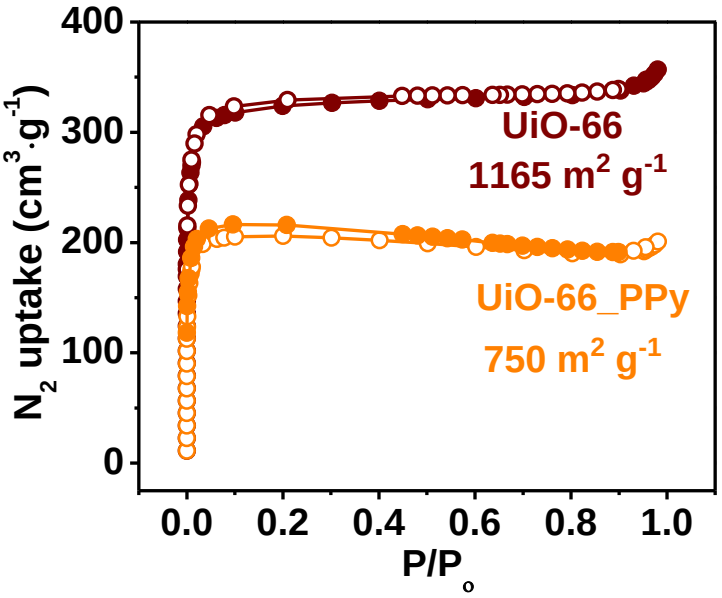

Figure 9: Nitrogen gas adsorption isotherms of UiO-66 (wine) and UiO-66_PPy (orange)

FESEM (Figure 10a and 10d) and HRTEM (Figure 10b and 10e) images reveal that both UiO-66 and UiO-66_PPy have an irregular spherical morphology. We do not observe any growth of polymer chains on the surface of the UiO-66_PPy, thus complementing the gas adsorption analysis of the formation of PPy chains inside the nanochannels. Elemental mapping of UiO-66_PPy showed a uniform distribution of nitrogen throughout the framework further confirming the presence of polypyrrole throughout the framework (Figure 10c). We also see the presence of Chlorine in UiO-66_PPy suggesting Cl^- ions act as dopants in the system to maintain the charge neutrality of the polymers formed (Figure 10f).[28]

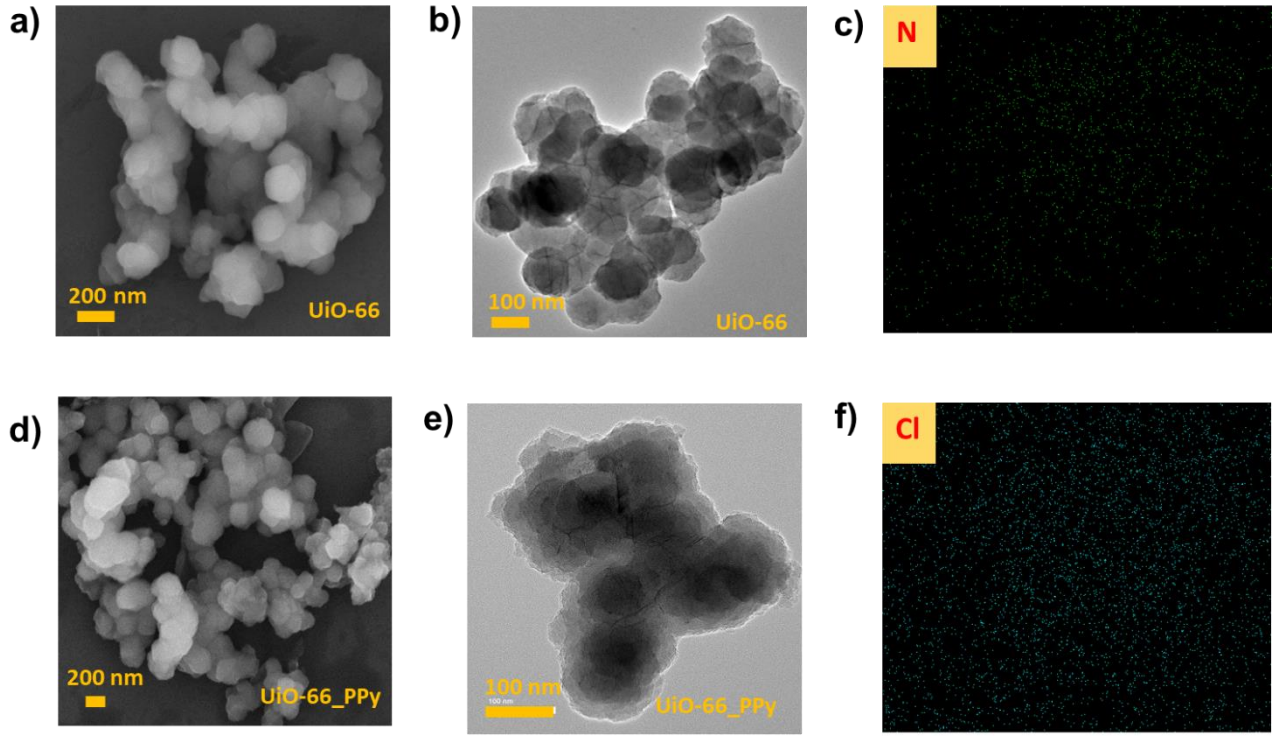

Figure 10: FESEM images of (a) UiO-66 (d) UiO-66_PPy and HRTEM images of (b) UiO-66 (e) UiO-66_PPy showing retention of morphology. Elemental mapping showing a uniform distribution of (c) Nitrogen and (f) Chlorine in UiO-66_PPy from FESEM and EDXS

Polypyrrole exists in three states, neutral state, polaron state and bipolaron state (Figure 11a). It is reported from electrochemical studies that the “redox potential for polymerization of pyrrole is always greater than doping of neutral pyrrole. Hence oxidative polymerization always leads to the formation of doped polymers chains”.[28] The polaron and bipolaron states occur due to this doping of the polymer, which in turn reduce the band gap in polypyrrole, making them conducting (Figure 11b). This is also evident from the Solid State UV-Vis spectra where we see a broad bipolaron band starting from ~ 400 nm for both UiO-66 and the bulk PPy which is absent in UiO-66 (Figure 11c). [29]

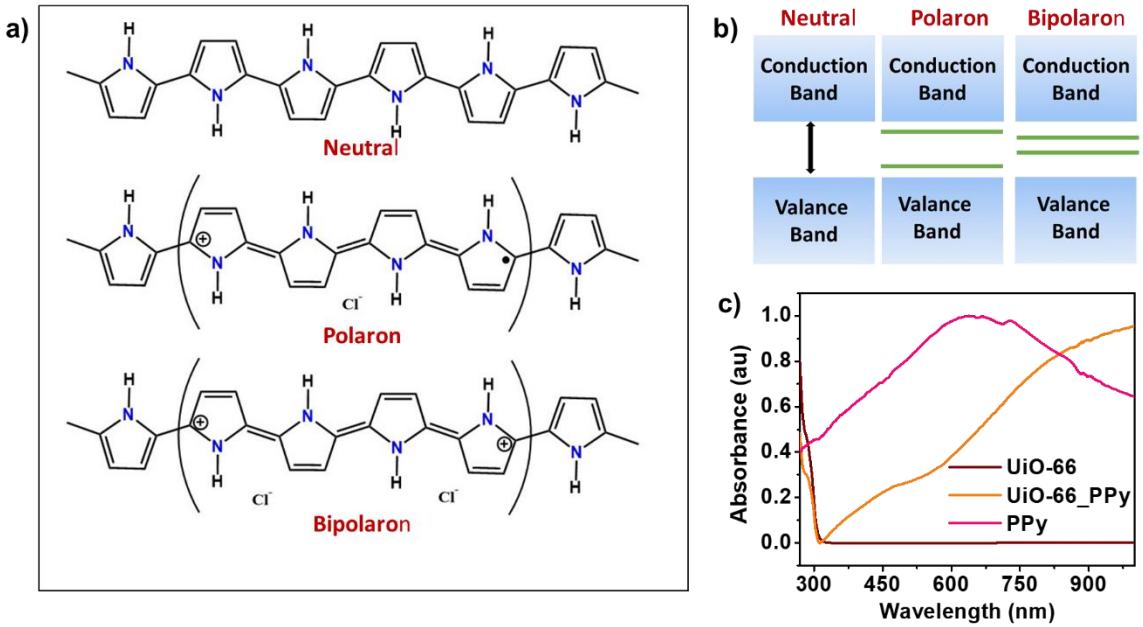

Figure 11: Structure of neutral, polaron and bipolaron states of PPy (b) band structure of PPy: left – neutral, centre – polaron and right – bipolaron states of PPy (c) Solid state UV-Vis of UiO-66 (wine), UiO-66_PPy (orange) and bulk PPy (pink)

3.2 Electrical Conductivity

After successful incorporation of polymer chains inside UiO-66, we tested its electrical conductivity. The conductivity studies were performed on pressed pellet by both DC and AC setups using Four-Probe, Two-probe and Electrochemical Impedance Spectroscopy

(EIS). We were able to reproduce the value in all the three types of measurements consistently. UiO-66 being insulating in nature exhibits conductivity value of ~10^{-8} S/cm.[30] On the other hand conductivity measurements carried out using Four-Probe technique (Figure 12a) give a value of ~1.9 x 10^{-2} S/cm for UiO-66_PPy nanocomposite – a million-fold increase. Two probe measurements (Figure 12b), as well as Nyquist data (Figure12c), also reveal similar values i.e. ~6.9 x 10^{-2} S/cm and ~7.6 x 10^{-2} S/cm respectively. Temperature-dependent conductivity studies were also carried out and it is observed that the conductivity increases with increase in temperature, which is a feature of a typical semiconductor. The activation energy was calculated by the following equation[31]:

$$\rho = A\, exp \frac{Ea}{KT} \qquad \text{(Eq. 1)}$$

where, ρ = resistivity, A = constant, E_a = activation energy, K = Boltzmann constant, and T = temperature. The activation energy calculated from Arrhenius plot is found to be 0.1eV (Figure 12d).

The enhancement in the electrical conductivity of the nanocomposite is primarily due to the interaction between the host framework and the highly oriented and doped Polypyrrole chains incorporated inside it, which effectively reduce the band gap in UiO-66 and thus help in the efficient transport of electrons. To confirm that there is indeed a synergistic interaction of the polymer with the aromatic ligands in the host framework, we measured the conductivity of the mechanical mixture of UiO-66 and bulk Polypyrrole. The conductivity is ~5.4 x 10^{-6} S/cm, much lower than the nanocomposite (Figure 11a-inset). This reduced value for the mechanical mixture is a clear indication that the enhancement in the electrical conductivity is a result of the host-guest interactions in the framework.

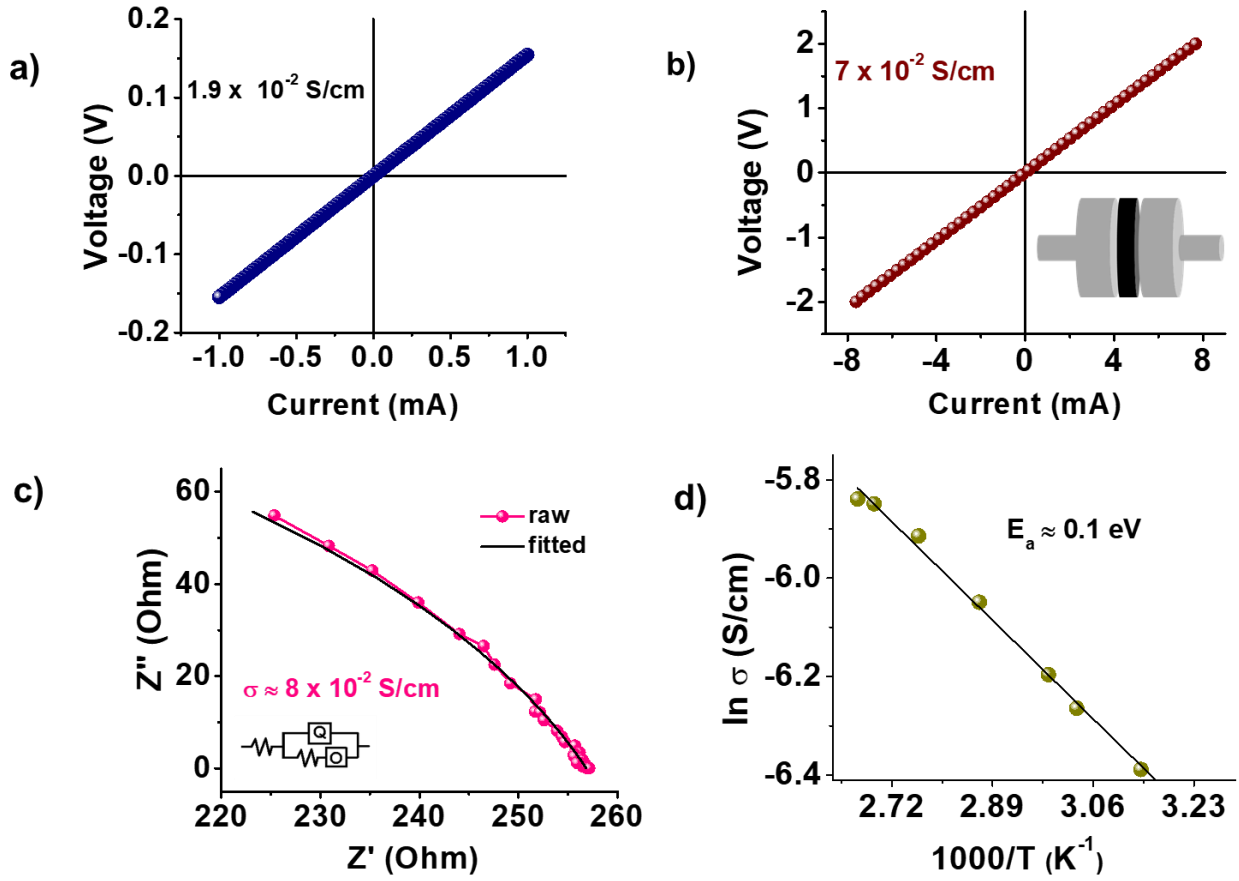

Figure 12: Electrical conductivity of UiO-66_PPy (a) Four-Probe: inset- Electrical conductivity of mechanical mixture and schematic of four-probe, (b) Two-Probe: inset- Schematic of Two-Probe and (c) Nyquist Plot. (d) Arrhenius Plot

3.3 Thermal Conductivity

Thermoelectric materials are of high desirability in the present day because they are able to convert heat into electricity. Owing to their porous nature, MOFs are able to scatter phonons effectively and thus are poor thermal conductors.[32] Additionally, as discussed in the introduction, conducting polymers are also thermally insulating. So the enhanced electrical conductivity and a lower thermal conductivity of the UiO-66_PPy nanocomposite would result in a potential material for such applications. With this in mind, we carried out thermal conductivity measurements on UiO-66 and UiO-66_PPy. Thermal conductivity

measurements were done on activated pressed pellets by using Laser flash Analysis (LFA) technique. The value was calculated using the following equation:

$$\kappa = C_P \times D \times \rho \quad \text{(Eq. 2)}$$

Where C_p is the specific heat capacity of the material, D is the thermal diffusivity and ρ is the density of the pellet. Specific heat capacity (C_p) was calculated from Differential Scanning Calorimetry (DSC). The following equation was used to calculate C_P[31]:

$$C_P = \frac{\Delta H}{\mathrm{m}\Delta T} \quad \text{(Eq. 3)}$$

where ΔH is the magnitude of heat flow, m is the mass of the sample and ΔT is the rate of change of temperature.[33] Room temperature value of specific heat capacity was taken into account for thermal conductivity calculations (Figure 13a).

Thermal conductivity is a result of two types of contributions: K_l and K_e where K_l and K_e are lattice and electronic contributions respectively. Due to the insulating nature of UiO-66, electronic contribution to the thermal conductivity can be considered negligible. The lattice contribution of thermal conductivity arises due to the porous nature of UiO-66 which is able to scatter phonons effectively. This results in a low value of thermal conductivity of ~0.86 W/mK. In the case of UiO-66_PPy, due to the enhanced electrical conductivity, one would expect a higher thermal conductivity. However, as there is still a significant amount of vacant space present in the pores of the nanocomposite, the lattice contribution to thermal conductivity still dominates. Additionally, conducting polymers, Polypyrrole, in this case, have shorter intrinsic phonon mean free path, making it thermally insulating. Reported values for thermal conductivity of Polypyrrole vary from ~0.17 W/mK to ~0.02 W/mK.[34] For UiO-66_PPy nanocomposite, we observe a lowered thermal conductivity value of ~0.46 W/mK (Figure 13b). This can be explained by the fact that the combined effect of low values for both the framework and the polymer chains as well as the porous nature of the nanocomposite results in the overall reduction of the thermal conductivity.

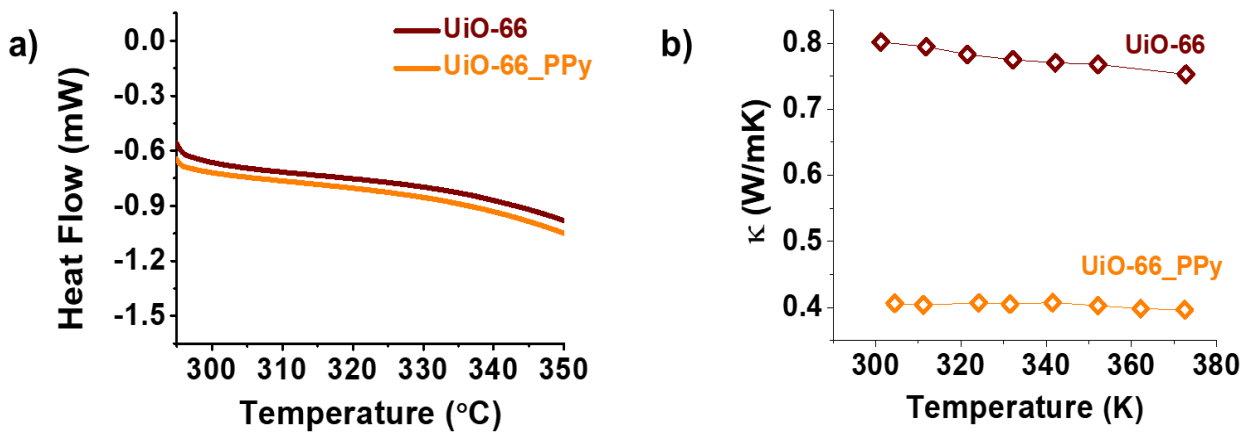

Figure 13: (a) DSC plot for UiO-66 and UiO-66_PPy (b) thermal conductivity of UiO-66 and UiO-66_PPy

In a nutshell, we have successfully enhanced the electrical conductivity and modulated the thermal conductivity of the nanocomposite. Additional experiments need to be performed to measure the Seebeck Coefficient and finally the thermoelectric figure of merit.

3.4 Supercapacitor Applications

The ever-growing demand for consumption of energy calls for new and effective ways to store and utilize energy. With the non-renewable sources of energy being overused, in the current scenario, they are expected to exhaust in the near future. Renewable energy, on the other hand, is abundant but is not available all the time and the distribution is not uniform geographically, thus, it needs to be stored. Consequently, energy storage devices are of utmost importance to meet energy demands. Batteries, fuel cells, capacitors and supercapacitors are some of the devices presently used for this purpose. Among these, supercapacitors represent an important class of energy storage devices that bridge the gap between batteries and capacitors to give optimal energy and power density.[35]

Although there have been some reports about conducting MOF based supercapacitors,[36] MOF-Conducting Polymer nanocomposite based supercapacitors are yet to be fully explored. Owing to the retained porosity and the enhanced electrical conductivity, we decided to test the material for supercapacitor applications. The supercapacitors were

tested in both liquid and solid state configurations (Figure 14a and 14b). Electrochemical measurements in the liquid and solid state configurations were carried out in 0.5 M H_2SO_4 and 10 wt% polymer gel electrolyte, respectively. Electrochemical techniques such as Cyclic Voltammetry (CV), Charge – Discharge (CD) and Electrochemical Impedance Spectroscopy (EIS) were used to evaluate the supercapacitor performance.

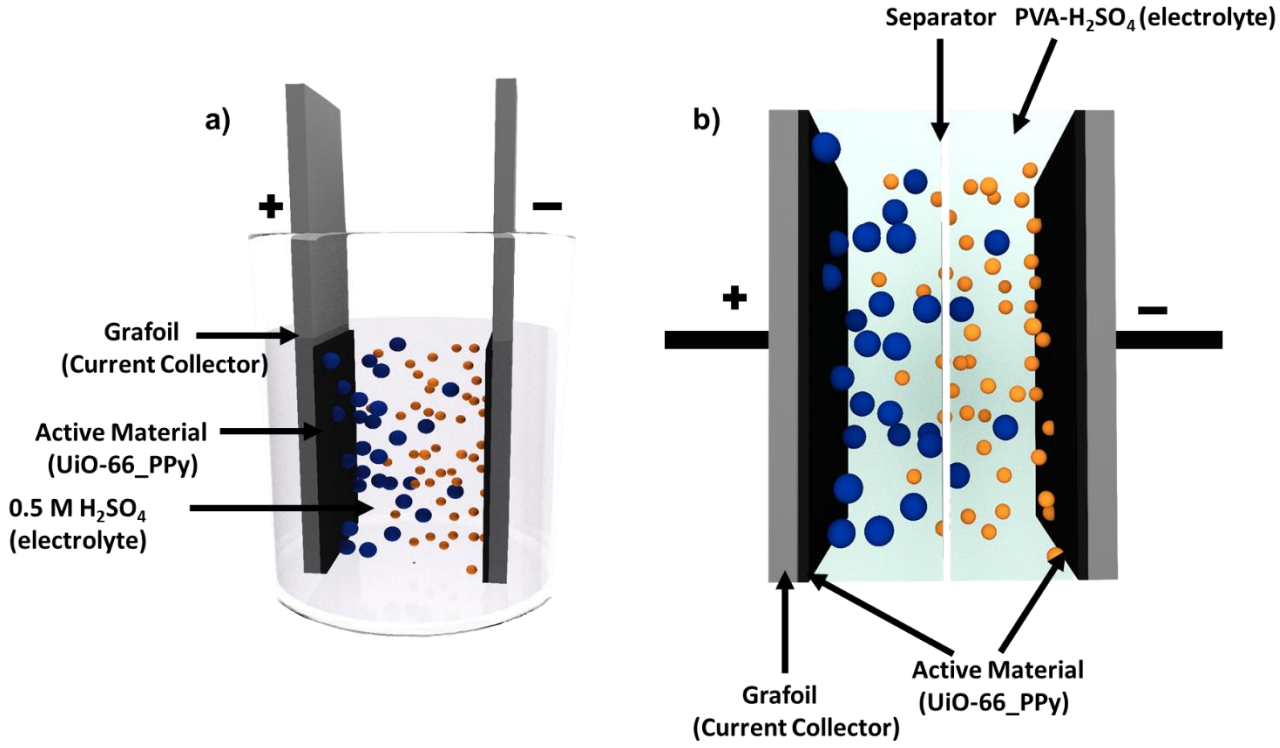

Figure 14: Schematic of (a) liquid state and (b) solid state assembly of supercapacitor

The almost rectangular CV curve in both the solid and liquid state configurations of the supercapacitors is indicative of the Electrical Double Layer Capacitance (EDLC) feature of the supercapacitor (Figure 15a and 15d). This is further corroborated by the triangular feature in the charge-discharge curves. The ever so slight deviation from the triangular curves in the CD could be due to the presence of redox-active doped Polypyrrole chains in the framework (Figure 15d and 15e). Additional three electrode measurements need to be done to probe the presence pseudo capacitive contribution to the overall capacitance, if any. In the Nyquist plot, the semicircle at higher frequency indicates the

charge transfer resistance in the system which is comprised of electrolyte resistance, electrode resistance, and the contact resistance between the electrode and current collector. The vertical line at a lower frequency is due to the ion transport resistance or the diffusion resistance.[37] From the Nyquist plots (Figure 15c and 15f) we can see a very small semicircle in both the solid and liquid configurations, indicating low charge transfer resistance of the system. The value for the both the systems is ~3 Ω, which suggests a high mobility of charge carriers.

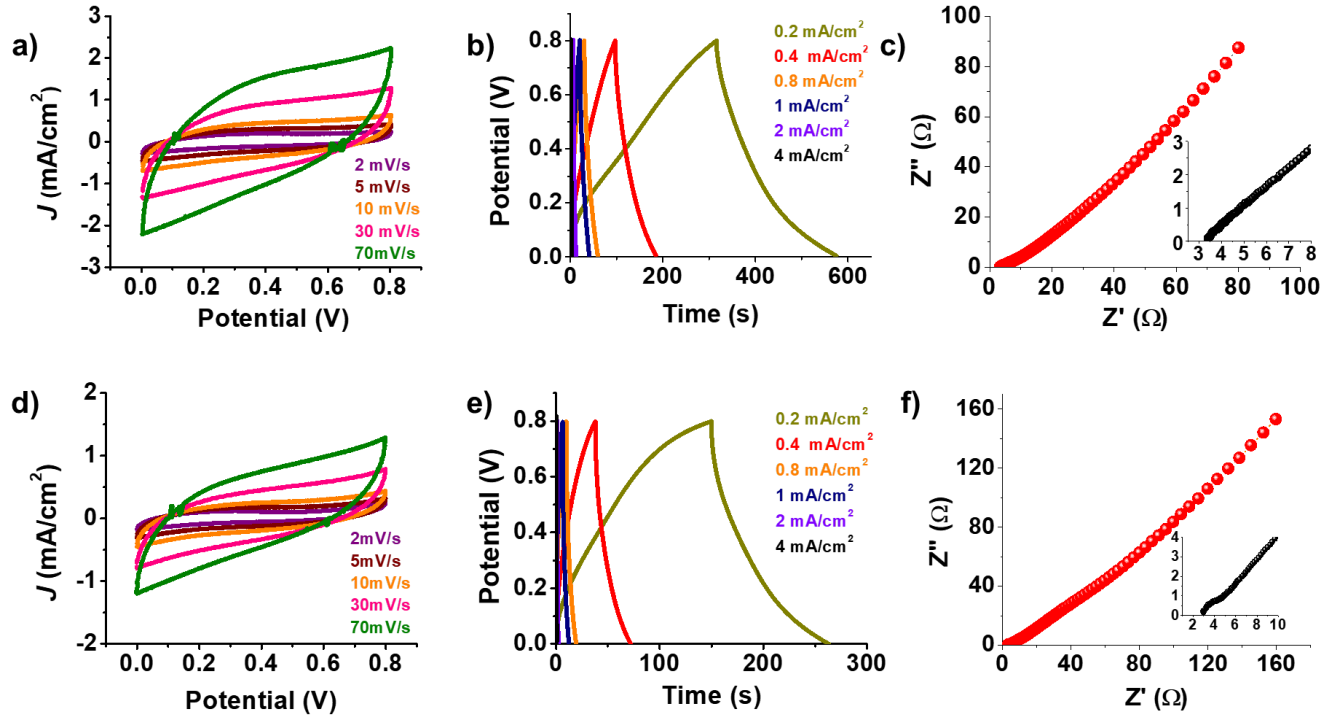

Figure 15: Electrochemical characterization of UiO-66_PPy: Upper panel – (a) CV (b) CD and (c) Nyquist in liquid state; bottom panel – (d) CV (e) CD and (f) Nyquist in solid state configuration

We calculated the areal and gravimetric resistance from the Charge-Discharge curves at different current densities. While the liquid state system gives areal capacitance of ~ 130 mF/cm^2 (Figure 16a) at current density of 0.2mA/cm^2, in the solid-state configuration, this value is ~ 60 mF/cm^2 (Figure 16b). This reduction in the value can be attributed to the lower mobility of the ions in the solid state matrix where a polymer gel electrolyte is used

as opposed to aqueous H_2SO_4 in the liquid configuration.[38] Nonetheless, these values indicate a significant improvement in the capacitance of the framework with only ~15 wt% loading of the conducting polymer. The performance can be further increased by varying the mass loading of the active material.

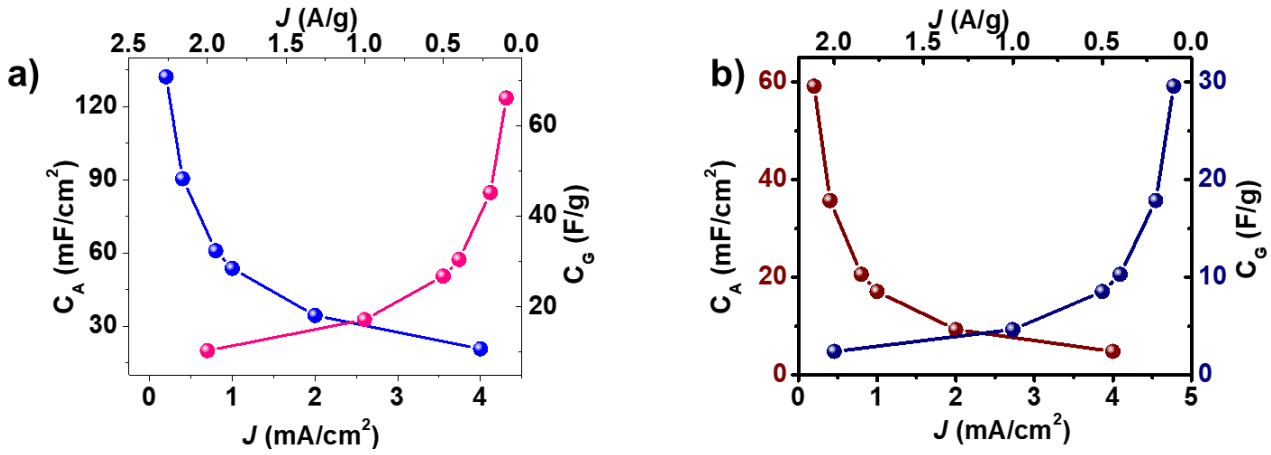

Figure 16: Plot for current specific capacitance vs current density (C_A and C_G) of UiO-66_PPy for (a) liquid state and (b) solid state configuration

Conducting polymers, composed of organic backbone, degrade after a couple of hundred cycles. This is due to the irreversible changes that occur in the structure of the polymers during the charge-discharge cycles, resulting in the collapsing of the structure.[39] Interestingly, UiO-66_PPy nanocomposite exhibits excellent cycling stability in both the liquid state and solid state configurations (Figure 17a and 17b). We observe that the material does not degrade up to over ten thousand cycles, with negligible loss in capacity in both the cases.

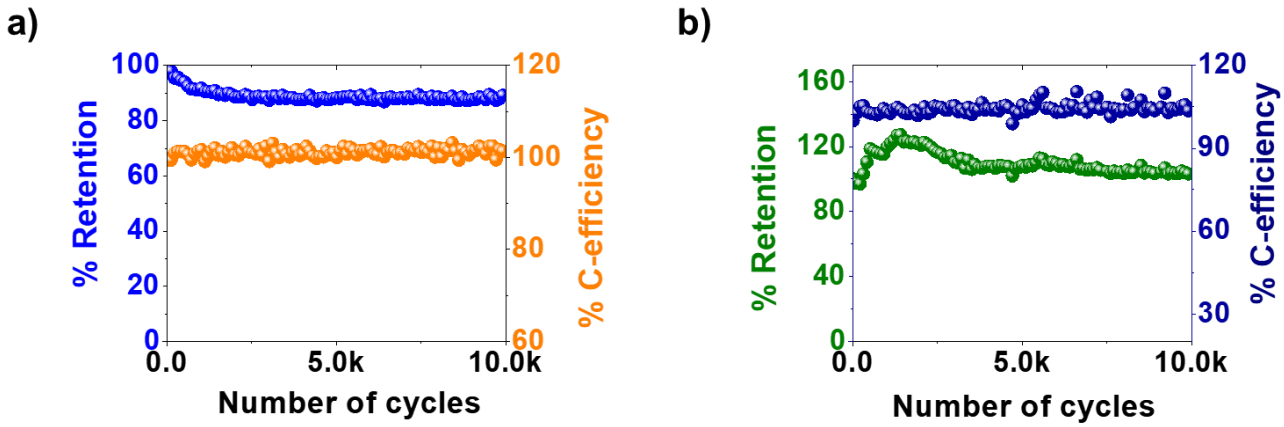

Figure 17: Cycling stability of UiO-66_PPy for (a) liquid state and (b) solid state configuration.

Further improvements in the capacity can be done by varying the mass loading of the active material as well as carrying out the measurements in organic electrolytes which allow the use of higher potential windows.

4. Conclusions

By using in-situ polymerization technique within the confined nano-spaces of the Metal-Organic Framework, we have successfully synthesized a porous, semiconducting MOF- Conducting Polymer nanocomposite which exhibits enhanced electrical conductivity by ~6 orders of magnitude as compared to the pristine MOF with ~15 wt% loading of the conducting polymer. Synergistic interaction between the conjugated polymers and the π electron cloud of the organic linker was understood as the primary reason for enhancement in electrical conductivity. Owing to the retained porosity of this nanocomposite, the thermal conductivity measurements reveled a low value of ~0.4 W/mK for the nanocomposite. Additionally, supercapacitor fabricated using the nanocomposite exhibited specific capacitance of ~130 mF/cm^2 and ~100 % retention up to over 10k cycles. This work offers a new direction in the field of porous semiconducting nanocomposites, which can have potential applications in the development of new energy storage systems.

5. References

(1) Li H, Eddaoudi M, O'Keeffe M, et al. Design and Synthesis of an Exceptionally Stable and Highly Porous Metal-Organic Frameworks. *Nature* **1999**, *402*, 276–279.

(2) Thomas-hillman, I.; Laybourn, A.; Kingman, S. W.; Dodds, C. Realising the Environmental Benefits of Metal – Organic Frameworks : Recent Advances in Microwave Synthesis. J. Mater. Chem. A, **2018**, 11564–11581

(3) Furukawa, H.; Furukawa, H.; Cordova, K. E.; Keeffe, M. O.; Yaghi, O. M. The Chemistry and Applications of Metal-Organic Frameworks. Science, **2013**, 341, 123044-123056

(4) Hendon, C. H.; Tiana, D.; Walsh, A. Conductive Metal – Organic Frameworks and Networks : Fact or Fantasy? Phys. Chem. Chem. Phys., **2012**, 14, 13120–13132

(5) D Shirakawa, H.; Louis, E, J.; Macdiarmid, A. G.; Chiang, C. K.; Heeger, A. J. Synthesis of Electrically Conducting Organic Polymers : Halogen Derivatives of Polyacetylene, $(CH)_x$. J.C.S. Chem. Comm. **1977**, 578, 578–580.

(6) Chiang, C. K..; Fincher, C. B Jr.; Park, Y. W.; Heeger, A. J.; Shirakawa, H.; Louis E. J.; Gau S. C.; MacDiarmid, A. G. Electrical Conductivity in Doped Polyacetylene. PHYSICAL REVIEW LETTERS, **1977**, 39, 1098–1101

(7) Winkler, K.; Zo, M. W. Structure, Electrochemical Properties and Capacitance Performance of Polypyrrole Electrodeposited onto 1-D Crystals of Iridium Complex. **2015**, *300*, 472–482

(8) Yue, R.; Xu, J. Poly (3,4-Ethylenedioxythiophene) as Promising Organic Thermoelectric Materials : A Mini-Review. *Synth. Met.* **2012**, *162*, 912–917

(9) D Dhara, B.; Nagarkar, S. S.; Kumar, J.; Kumar, V.; Jha, P. K.; Ghosh, S. K.; Nair, S.; Ballav, N. Increase in Electrical Conductivity of MOF to Billion-Fold upon Filling the Nanochannels with Conducting Polymer. *J. Phys. Chem. Lett.* **2016**, *7*, 2945–2950

(10) Sun, L.; Campbell, M. G.; Dinca, M. Electrically Conductive Porous Metal – Organic Frameworks Angewandte. **2016**, 55 3566–3579

(11) Takaishi, S.; Hosoda, M.; Kajiwara, T.; Miyasaka, H.; Yamashita, M.; Nakanishi, Y.; Kitagawa, Y.; Yamaguchi, K.; Kobayashi, A.; Kitagawa, H. Electroconductive Porous Coordination Polymer $Cu[Cu(Pdt)_2]$ Composed of Donor and Acceptor Building Units. Inorganic Chemistry, **2009**, 48, 9048-9050

(12) Kobayashi, Y.; Jacobs, B.; Allendorf, M. D.; Long, J. R. Conductivity , Doping , and Redox Chemistry of a Microporous Dithiolene-Based Metal - Organic Framework. **2010**, No. 5, 4120–4122.

(13) Framework, M.; Talin, A. A.; Centrone, A.; Ford, A. C.; Foster, M. E.; Stavila, V.; Haney, P.; Kinney, R. A.; Szalai, V.; Gabaly, F. El; et al. Tunable Electrical Conductivity in Metal-Organic Framework Thin-Film Devices. Science **2014**, *343*, 66–70

(14) Wang, Q. X.; Zhang, C. Y. Oriented Synthesis of One-Dimensional Polypyrrole Molecule Chains in a Metal-Organic Framework. *Macromol. Rapid Commun.* **2011**, *32*, 1610–1614.

(15) Aliev, S. B.; Samsonenko, D. G.; Maksimovskiy, E. A., Fedorovskaya,E. O.; Sapchenko, S. A. and Fedin. V .P. Polyaniline-intercalated MIL-101: selective CO2 sorption and supercapacitor properties. New J. Chem. **2016**, 40, 5306–5312.

(16) Wang, T.; Farajollahi, M.; Henke, S.; Zhu T, Bajpe, S. R.; Sun, S.; Barnard, J. S.; Lee, J S.; Madden, J. D. W.; Cheetham, A. K.; Smoukov, S. K. Functional Conductive Nanomaterials via Polymerisation in Nano-Channels: PEDOT in a MOF. Mater. Horiz. **2017**, 4, 64-71

(17) Maclean, M. W. A.; Kitao, T.; Suga, T.; Mizuno, M.; Seki, S.; Uemura, T.; Kitagawa, S. Communications Metal – Organic Frameworks Unraveling Inter- and Intrachain Electronics in Polythiophene Assemblies Mediated by Coordination Nanospaces. **2016**, 55, 708–713.

(18) Le Ouay, B.; Uemura, T. Polymer in MOF Nanospace: From Controlled Chain

Assembly to New Functional Materials. *Isr. J. Chem.* **2018**, 58,1–16.

(19) Luo, T.; Whang, W.; Chen, C.; Lu, K. Zr-MOF/Polyaniline Composite Films with Exceptional Seebeck Coefficient for Thermoelectric Material Applications. **2018**, 11, 3400-3406

(20) Shao, L.; Wang, Q.; Ma, Z.; Ji, Z.; Wang, X.; Song, D.; Liu, Y.; Wang, N. A High-Capacitance Fl Exible Solid-State Supercapacitor Based on Polyaniline and Metal-Organic Framework (UiO-66) Composites. *J. Power Sources* **2018**, *379*, 350–361.

(21) Cavka, J. H.; Jakobsen, S.; Olsbye, U.; Guillou, N.; Lamberti, C.; Bordiga, S.; Lillerud, K. P. A New Zirconium Inorganic Building Brick Forming Metal Organic Frameworks with Exceptional Stability. *J. Am. Chem. Soc.* **2008**, 130, 13850–13851

(22) Desai, A. V; Samanta, P.; Manna, B.; Ghosh, S. K. Aqueous Phase Nitric Oxide Detection by an Amine-Decorated Metal-organic Framework. **2015**, 51, 6111–6114

(23) Boutry, C. M; Gerber-Horler, Hierold C. Electrically Conducting Biodegradable Polymer Composites (Polylactide-Polypyrrole and Polycaprolactone-Polypyrrole) for Passive Resonant Circuits. POLYMER ENGINEERING AND SCIENCE. **2013**, 1196-1208

(24) Hajek, J.; Caratelli, C.; Demuynck, R.; Vanduyfhuys, L.; Waroquier, M.; Speybroeck, V. Van. On the intrinsic dynamic nature of the rigid UiO-66 metal–organic framework. Chem. Sci. **2018**, *9*, 2723–2732

(25) Driscoll, D. M.; Troya, D.; Usov, P. M.; Maynes, A. J.; Morris, A. J.; Morris, J. R. Characterization of Undercoordinated Zr Defect Sites in UiO-66 with Vibrational Spectroscopy of Adsorbed CO. *J. Phys. Chem. C* **2018**, *122*, 14582–14589.

(26) Liang, X.; Wen, Z.; Liu, Y.; Wang, X.; Zhang, H.; Wu, M.; Huang, L. Preparation and Characterization of Sulfur – Polypyrrole Composites with Controlled Morphology as High Capacity Cathode for Lithium Batteries. *Solid State Ionics*

2011, *192*, 347–350.

(27) Zhao, W.; Zhang, C.; Yan, Z.; Zhou, Y.; Li, J. Performance Evaluation of UiO-66 Analogues as Stationary Phase in HPLC for the Separation of Substituted Benzenes and Polycyclic Aromatic Hydrocarbons. **2017**, *101*, 1–13.

(28) Miyata, S.; Techagumpuch, A. Chemical synthesis of highly electrically conductive Polypyrrole, Synthetic Metals, **1989**, 31, 311 - 318

(29) Choudhary, M.; Islam, U.; Witcomb, M. J.; Mallick, K. In situ generation of a high-performance Pd-polypyrrole composite with multi-functional catalytic properties Dalton Transactions**. 2014,** 43, 6396–6405

(30) Musho, T. D.; Yasin, A. S. Ab-Initio Study of the Electron Mobility in a Functionalized UiO-66 Metal Organic Framework. *J. Electron. Mater.* **2018**, *47* , 3692–3700.

(31) Menzinger, B. M. The Meaning and Use of the Arrhenius Activation Energy. **1969**, *8*, 438–444.

(32) Babaei, H.; McGaughey, A J. H.; Wilmer, C. E.; Effect of pore size and shape on the thermal conductivity of metal-organic frameworks. *Chemical Science*. **2016**, 8, 583–589.

(33) Zhou, S-Q.; Ni, R. Measurement of the Specific Heat Capacity of Water-Based Nanofluid. Appl. Phys. Lett. **2008**, 92, 1–4.

(34) Culebras, M.; Uriol, B.; Gomez, C. M.; Cantarero, A. Controlling the Thermoelectric Properties of Polymers : Application to PEDOT and Polypyrrole. Phys.Chem.Chem.Phys. **2015**, 17, 15140–15145.

(35) Ko, R.; Carlen, M. Principles and Applications of Electrochemical Capacitors. **2000**, *45*, 2483–2498.

(36) Feng, D.; Lei, T.; Lukatskaya, M. R.; Park, J.; Huang, Z.; Lee, M.; Shaw, L.; Chen, S.; Yakovenko, A. A.; Kulkarni, A.; et al. Volumetric and Areal Capacitance. *Nat. Energy* **2018**, **3**, 30–36

(37) Mei, B.; Munteshari, O.; Lau, J.; Dunn, B.; Pilon, L. Physical Interpretations of Nyquist Plots for EDLC Electrodes and Devices. J. Phys. Chem. C **2018**, 122, 194−206.

(38) Khalid, M.; Tumelero, M. A.; Pasa, A. A. Asymmetric and Symmetric Solid-State Polyaniline – Carbon Nanotube Framework. RSC Adv. **2015**, 5, 62033–62039.

(39) Liu, C.; Yu, Z.; Neff, D.; Zhamu, A.; Jang, B. Z. Graphene-Based Supercapacitor with an Ultrahigh Energy Density. Nano Lett. **2010,** 10, 4863–4868.